

Lamellar Phase Separation and Dynamic Competition in $\text{La}_{0.23}\text{Ca}_{0.77}\text{MnO}_3$

J. Tao,¹ D. Niebieskikwiat,² M. B. Salamon,² and J. M. Zuo¹

¹Department of Materials Science and Engineering, University of Illinois at Urbana-Champaign, Urbana, Illinois 61801, USA

²Department of Physics, University of Illinois at Urbana-Champaign, Urbana, Illinois 61801, USA

(Received 10 September 2004; published 14 April 2005)

We report the coexistence of lamellar charge-ordered (CO) and charge-disordered (CD) domains, and their dynamical behavior, in $\text{La}_{0.23}\text{Ca}_{0.77}\text{MnO}_3$. Using high-resolution transmission electron microscopy (TEM), we show that below $T_{\text{CD}} \sim 170$ K a CD-monoclinic phase forms within the established CO-orthorhombic matrix. The CD phase has a sheetlike morphology, perpendicular to the \mathbf{q} vector of the CO superlattice (a axis of the $Pnma$ structure). For temperatures between 64 and 130 K, both the TEM and resistivity experiments show a dynamic competition between the two phases: at constant T , the CD phase slowly advances over the CO one. This slow dynamics appears to be linked to the magnetic transitions occurring in this compound, suggesting important magnetoelastic effects.

DOI: 10.1103/PhysRevLett.94.147206

PACS numbers: 75.47.Lx, 61.14.Lj, 61.20.Lc, 75.60.Ch

Decades of research have yet to allow us to completely understand the full range of ordered phases that occur in the $A_{1-x}A'_x\text{MnO}_3$ perovskites ($A = \text{La, Pr, Nd}$ and $A' = \text{Ca, Sr, Ba}$) [1]. For $x \leq 0.5$, a complex competition occurs among ferromagnetic (FM), paramagnetic (PM), and charge-ordered (CO) antiferromagnetic (AFM) phases. In this regime, inhomogeneous phase separation (PS) gives rise to the well-known colossal magnetoresistance effect [2–4]. This regime has been widely studied and is reasonably well understood in terms of disorder-induced PS [3,5], which produces a fractal-like morphology of the coexisting domains [4].

Less well examined, and far richer, behavior is found for $x \geq 1/2$. In this region, electron microscopy and other spectroscopic tools find strong evidence for the appearance of charge ordering. The CO phases are characterized by the appearance of superlattice diffraction spots with a wave vector $q = 1 - x$, corresponding to real-space “stripes” with a period $a/(1 - x)$, perpendicular to the a axis of the orthorhombic perovskite structure ($Pnma$ space group) [6]. As the temperature is lowered below the CO transition at T_{CO} , neutron scattering shows the emergence of AFM ordering of the Mn moments at $T_{\text{N}} < T_{\text{CO}}$ [7]. Because charge is discrete, we would expect a robust CO phase to occur at rational values of x , i.e., at $x = 1/2, 2/3, 3/4 \dots$. Indeed, for $x = 2/3$ a fully commensurate CO-AFM state appears. Surprisingly, Pissas and Kallias [8] reported recently that the $x = 3/4$ state is unstable, phase separating into a CO-AFM state similar to the $x = 2/3$ structure, and a C-type AFM phase not unlike that for $x = 0.80$ [9]. In this paper, we demonstrate that this PS is dynamic, and results in lamellar charge-disordered (CD) regions that grow in number and size below a charge disordering temperature T_{CD} . Both the structure of the lamellae, and the appearance of additional Bragg peaks indicate that this separation also involves a change in crystal structure. We monitor the evolution of the phases through time-dependent measurements of resistivity, magnetization,

and high-resolution transmission electron microscopy (TEM) images.

Our polycrystalline sample $\text{La}_{0.23}\text{Ca}_{0.77}\text{MnO}_3$ was prepared by the nitrate decomposition route, as described elsewhere [10], with a final sintering process at 1500°C for 24 h. *In situ* temperature dependent dark field electron imaging and electron diffraction were carried out using the JEOL 2010F (200 kV) transmission electron microscope under the experimental conditions previously described [11]. Magnetization (M) measurements as a function of temperature were performed using a commercial SQUID magnetometer. The M data were obtained by warming the

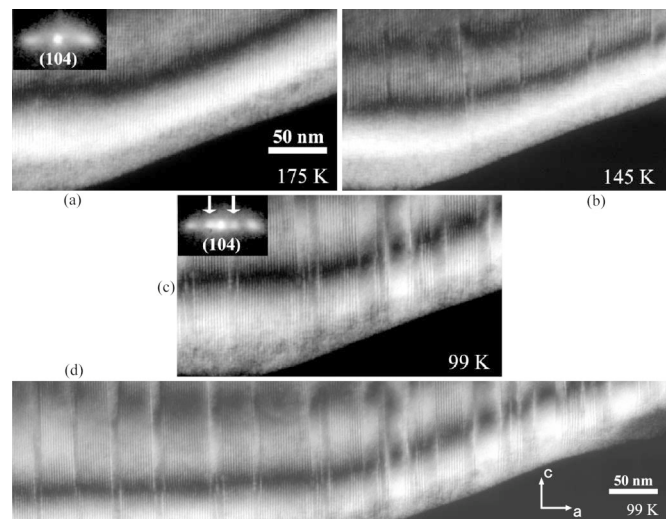


FIG. 1. (a) to (c) Temperature evolution of the dark field images of the same region of the sample. A large area view of the CO-CD phase separation at $T = 99$ K is shown in (d). The inset in (a) shows the two CO satellite reflections around the (104) fundamental peak ($T = 175$ K). The two additional reflections observed at $T = 99$ K [white arrows in the inset of part (c)] correspond to the CD phase and were indexed to a monoclinic structure.

sample in a magnetic field $H = 100$ Oe after zero-field-cooling (ZFC) and field-cooling (FC) processes from 300 K to 10 K. The resistivity (ρ) was measured by the usual four probe method.

Figure 1 shows the temperature driven evolution of the microstructure of a selected region of the sample, recorded by high-resolution dark field imaging using a fundamental reflection and the two corresponding CO superlattice spots. At $T = 175$ K [Fig. 1(a)] the striplike contrast formed by the interference between these three reflections is evident [6,11]. In transport measurements, the onset of the CO phase is indicated by a pronounced increase of ρ , while the $M(T)$ curve shows a peak at the transition (see inset of Fig. 2). The occurrence of this peak was ascribed to the freezing of the double exchange interaction due to the localization of the charge carriers below T_{CO} (~ 220 K in our case). However, contrary to the nearly uniform CO phase present at 175 K, in Fig. 1(b) ($T = 145$ K) it can be seen that some nonstriped “bands” (sheets in 3D) nucleate inside the CO regions. The disappearance of the CO stripes indicates that these bands are undergoing a transition to a CD phase, which starts to occur at $T_{CD} \sim 170$ K. As the temperature is lowered the CD regions grow in both number and size, and the image in Fig. 1(c) at $T = 99$ K (the lowest achievable temperature for our TEM) exhibits a substantial amount of the CD phase. The picture presented in Fig. 1(d) shows a larger area ($\sim 0.6 \mu\text{m}$ wide) indicating that the appearance of this CD phase is not a local effect, but is spread throughout the sample with domain sizes ranging from ~ 10 to 30 nm wide.

Several important observations can be made from the images shown in Fig. 1. First of all, the CD phase cannot be attributed to a chemical segregation or composition variations in the sample. The CD domains occupy the same regions where the homogeneous CO phase was present at higher temperatures. Moreover, repetitions of the same experiment show similar images, but the CD areas do not always appear at the same locations in the sample; i.e., the CD phase is not pinned to defects.

Secondly, the morphology of the lamellar phase coexistence is striking. The minority CD domains appear as sheets embedded within the CO phase, where the domain walls separating both phases are nearly perpendicular to the a axis of the orthorhombic perovskite structure. This consideration indicates that, contrary to previous results in other phase separated manganites [3,5], random disorder hardly could be responsible for the coexistence of phases observed in $\text{La}_{0.23}\text{Ca}_{0.77}\text{MnO}_3$. In this kind of phase separation, the elastic energy must play a fundamental role in order to produce such smooth domain walls with their normals determined by the [100] propagation direction of the CO structural distortion.

In order to determine the nature of the CD phase we studied the electron diffraction pattern of the sample at $T = 175$ K [inset of Fig. 1(a)] and $T = 99$ K [inset of

Fig. 1(c)]. It can be observed that around the fundamental reflections [(104) is shown] the superlattice spots of the CO phase show up at both temperatures. These CO spots appear right below T_{CO} , with a wave vector $q \approx 0.23(1)$ indicative of the doping level $x \approx 0.77$. In addition to these spots, the white arrows in the inset of Fig. 1(c) signal the presence of another set of reflections near the strong fundamental one. These reflections are totally absent for $T > T_{CD}$, indicating that they are related to the CD phase. These satellite reflections were indexed to a monoclinic phase sharing the common a and b axes with the CO-orthorhombic phase, but with the c axis tilted by an angle of $\sim 1.3^\circ$ from the orthorhombic structure. The two spots at each side of the fundamental reflection correspond to different monoclinic domains with the positive and negative tilting angle.

Therefore, below T_{CD} we observe the coexistence of the CO-orthorhombic (CO-O) and CD-monoclinic (CD-M) phases. The observation of the secondary CD-M phase is consistent with neutron scattering measurements [8], where $\sim 25\%$ of the volume of $\text{La}_{1/4}\text{Ca}_{3/4}\text{MnO}_3$ samples was found to belong to the $P2_1/m$ monoclinic space group at low T . Also the temperature $T_{CD} \approx 170$ K coincides with the appearance of extra magnetic reflections in the neutron diffraction pattern. These reflections were associated to the monoclinic phase which adopts the C-type AFM structure [9].

In our magnetization curves (inset of Fig. 2) the proximity of the prominent “CO peak” hinders the observation of the AFM transition related to the appearance of the CD-M phase. However, the $M(T)$ data present some other curious features. As the temperature decreases, the splitting between the ZFC and FC curves becomes significant

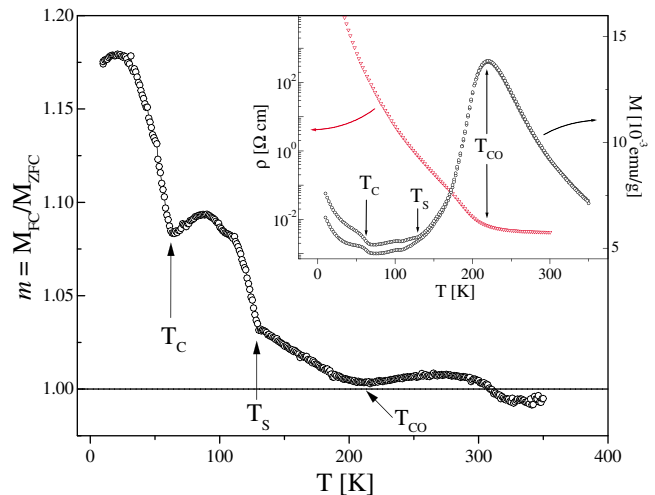


FIG. 2 (color online). Inset: zero-field-resistivity (left axis) and magnetization (right axis) as a function of temperature. M was measured with a magnetic field $H = 100$ Oe after ZFC and FC processes. Main panel: $m = M_{FC}/M_{ZFC}$ is the ratio between the magnetization obtained after FC and ZFC, respectively.

below $T_S \approx 130$ K, and at $T_C \approx 64$ K a small but clear magnetization increase occurs. While T_S indicates the PM to AFM transition of the CO phase, the weak FM moment showing up at T_C is related to the monoclinic phase [12]. Figure 2 plots the curve of the reduced magnetic moment $m(T) = M_{FC}/M_{ZFC}$, where M_{FC} and M_{ZFC} are the magnetization values for the FC and ZFC processes, respectively. At high temperature, as expected for a normal PM phase, the reduced moment remains close to $m = 1$ within less than 1% (this is within the reproducibility error). On the other hand, as soon as the CO phase is formed m starts to increase. Since immediately below T_{CO} the CO phase does not adopt any magnetic order, the value $m > 1$ indicates the presence of defects within the CO background with a “glassy” response to the application of a magnetic field. The other two magnetic transition temperatures, T_S and T_C , are characterized by abrupt breaks in $m(T)$.

Within the CO-CD phase coexistence regime, below $T_{CD} \sim 170$ K, an anomalous dynamic behavior sets in between $T_S \approx 130$ K and $T_C \approx 64$ K. Figure 3 presents ρ data as a function of time for selected temperatures, recorded over periods of ~ 3 hours. For each curve, the sample was warmed up to 300 K and then cooled back at 4 K/min and stabilized at the measuring temperature within ± 2 mK. For $T_S < T < T_{CO}$ the resistivity increases with time. This effect is present even above T_{CD} , indicating that it is not related to the phase coexistence but is a property of the CO-O phase itself. Moreover, we observed the same effect in the CO-O phase of $\text{La}_{1/3}\text{Ca}_{2/3}\text{MnO}_3$ samples, where the CD-M phase was not observed in the TEM studies [11]. For $x = 0.77$, the increase of resistivity

with time is correlated with an increase in the intensity of the CO superlattice reflections (not shown), which indicates that the CO phase is becoming more ordered with time [12]. This behavior supports the existence of mobile microscopic defects in the CO-O phase, which are responsible for the aforementioned glassy response observed in $m(T)$ for $T < T_{CO}$. The ability of these defects to migrate outside the CO volume provides the mechanism for the improvement of ordering with time.

In the inset of Fig. 3 we show the logarithmic relaxation rate $S = d(\log\rho)/d(\log t)$ as a function of temperature, obtained from the time interval between 10 and 20 min. The positive values of S for $T > T_S$ relate to the increase of ρ with time. A similar time evolution ($S > 0$) is observed for T below $T_C = 64$ K. Surprisingly, in the intermediate region $T_C < T < T_S$ the relaxation rate changes sign ($S < 0$) and the resistivity decreases with time. Remarkably, the changes in the dynamical behavior coincide with the magnetic transitions at T_S and T_C . In order to gain some insight on the dynamic properties of this compound we obtained dark field images of a given region of the sample at different times. As shown in Fig. 4, when the sample is cooled to $T = 99$ K (at approximately 4 K/min) the phase separation pattern evolves with time. Figure 4(a) shows that immediately after the sample is stabilized at 99 K the CD-M phase occupies a small part of the volume. However, some regions of the sample undergo a transition from the CO-O to the CD-M phase (see the framed region, for example), and the volume fraction of the latter keeps increasing with time. At 30 min after the temperature is reached [Fig. 4(d)] the CD-M phase occupies an appreciable fraction of the area of the image. Beyond

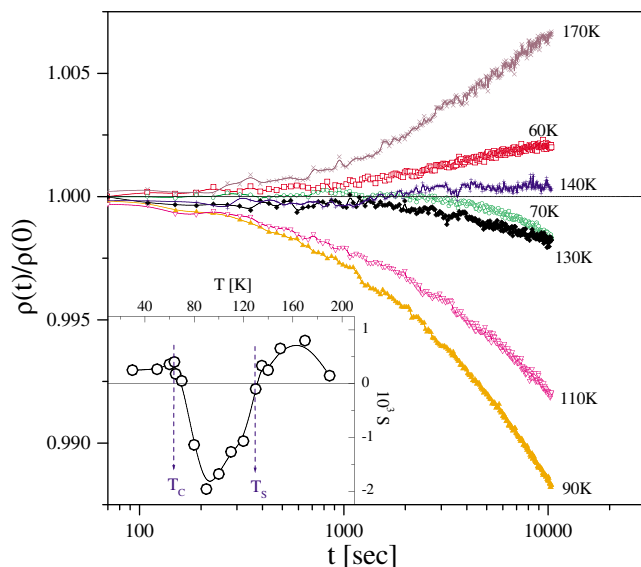


FIG. 3 (color online). Time dependence of the electrical resistivity of $\text{La}_{0.23}\text{Ca}_{0.77}\text{MnO}_3$ at different temperatures. Inset: logarithmic relaxation rate $S = d(\log\rho)/d(\log t)$ as a function of temperature, taken from the time interval 10 min $< t < 20$ min.

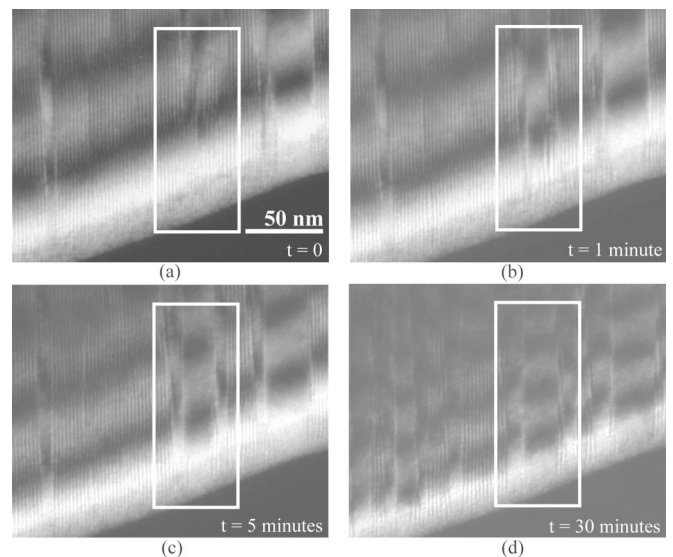


FIG. 4. Temporal evolution of the dark field images of the sample. (a) Initial stage; (b), (c), and (d) were taken after 1, 5, and 30 min, respectively. The frames show a region where the CD phase is expanding with time.

$t = 30$ min the relaxation becomes very slow, and no obvious change was observed in the images. It is worth mentioning that similar relaxation effects were also observed at $T = 115$ K. At $T = 125$ K the time evolution of the pattern is very slow and at $T = 135$ K ($> T_S$) it becomes unobservable. Thus, all these structural changes have an absolute correlation with the resistivity relaxation.

The above results present a consistent scenario of the complex dynamic competition between the CO and CD phases for T below T_S . It is well-known that a charge-ordered phase provides a strong insulating state due to the localized nature of the charge carriers on well-defined Mn sites. Differently, the particular C-type AFM structure of the CD-M phase consists of antiferromagnetically coupled FM chains, inside which the double exchange interaction [13] favors the delocalization of the charge carriers [9]. As a result, even though the AFM nature of the CD-M phase also produces an overall insulating state, the carriers' motion along these one-dimensional paths leads to a reduction of the resistivity. Therefore, contrary to the case of the upward relaxation, for $T < T_S$ the negative $d\rho/dt$ must be due to the slow growth of the CD-M phase in the CO-O matrix. For $T < 64$ K, the return of the relaxation rate towards positive values indicates that the motion of the boundaries between the two phases is stopped again.

A peculiar feature about the interplay between magnetic, electronic, and structural degrees of freedom in $\text{La}_{0.23}\text{Ca}_{0.77}\text{MnO}_3$ is that the occurrence of a magnetic phase transformation is able to induce a change in the dynamic properties of the phase coexistence. The new magnetic order that appears below $T_S \approx 130$ K triggers the motion of the domain walls that separate the CO-O and CD-M domains. At lower temperature, the appearance of a FM component is able to freeze this motion again, driving the system back to a static phase separated state. This behavior implies the existence of strong magnetoelastic effects [14]. Indeed, a magnetostrictive response was already observed [9] at the Néel temperature of the (orthorhombic) G-type AFM structure in $\text{La}_{0.12}\text{Ca}_{0.88}\text{MnO}_3$. This magnetic transition was also found to have an appreciable impact on the structural properties of the also present C-type AFM phase. It was previously argued that the large strain produced by the CO state on the borders of the domains greatly affects the physical properties of phase separated manganites, producing martensitic-like features [15]. In the case of our $\text{La}_{0.23}\text{Ca}_{0.77}\text{MnO}_3$ sample, a change in the magnetic structure of the coexisting phases would produce a change in the strain fields at the boundaries between them, thus affecting the delicate energy balance of the system and allowing (or precluding) the migration of the domain walls.

Summarizing, the close correlation between the high-resolution TEM images and the physical properties

allowed us to obtain a complete picture about the phase separated state in the $\text{La}_{0.23}\text{Ca}_{0.77}\text{MnO}_3$ manganite. Below the CO transition at $T_{\text{CO}} \sim 220$ K the high-resolution images show the typical CO stripes fully formed in the whole sample. However, on further cooling below $T_{\text{CD}} \sim 170$ K some non-CO laminated regions with a monoclinic structure form within the CO-orthorhombic matrix. The particular morphology of the charge-disordered domains and the simultaneity of magnetic and dynamic transitions observed at lower temperatures indicate that the CO-CD phase coexistence in this manganite must be driven by magnetoelastic effects rather than being dictated by disorder. The fundamental question that remains open is what is the real ground state of the electron doped manganites. For $x \approx 0.77$, contrary to the widely expected CO phase, the present results support a monoclinic C-type-AFM ground state. The realization of such phase seems to be only impeded by the inability of the domain walls to move out of the sample fast enough, stopped by the strain fields induced by the high-temperature CO phase.

This material is based upon work supported by the U.S. Department of Energy, Division of Materials Sciences under Grant No. DEFG02-91ER45439, through the Frederick Seitz Materials Research Laboratory and the Center for Microanalysis of Materials at the University of Illinois at Urbana-Champaign. J. T. was supported by DOE under Grant No. DEFG02-01ER45923.

-
- [1] M. B. Salamon and M. Jaime, *Rev. Mod. Phys.* **73**, 583 (2001); J. M. D. Coey *et al.*, *Adv. Phys.* **48**, 167 (1999).
 - [2] S. Jin *et al.*, *Science* **264**, 413 (1994).
 - [3] E. Dagotto *et al.*, *Phys. Rep.* **344**, 1 (2001).
 - [4] M. Fäth *et al.*, *Science* **285**, 1540 (1999).
 - [5] A. Moreo *et al.*, *Phys. Rev. Lett.* **84**, 5568 (2000); M. B. Salamon *et al.*, *ibid.* **88**, 197203 (2002); D. Niebieskikwiat *et al.*, *Phys. Rev. B* **63**, 212402 (2001).
 - [6] C. H. Chen *et al.*, *J. Appl. Phys.* **81**, 4326 (1997); S. Mori *et al.*, *Nature (London)* **392**, 473 (1998).
 - [7] P. G. Radaelli *et al.*, *Phys. Rev. B* **59**, 14440 (1999); M. T. Fernández-Díaz *et al.*, *ibid.* **59**, 1277 (1999).
 - [8] M. Pissas and G. Kallias, *Phys. Rev. B* **68**, 134414 (2003).
 - [9] C. D. Ling *et al.*, *Phys. Rev. B* **68**, 134439 (2003).
 - [10] D. Niebieskikwiat *et al.*, *Phys. Rev. B* **66**, 134422 (2002).
 - [11] J. Tao and J. M. Zuo, *Phys. Rev. B* **69**, 180404 (2004).
 - [12] D. Niebieskikwiat *et al.* (to be published).
 - [13] C. Zener, *Phys. Rev.* **82**, 403 (1951).
 - [14] K. H. Ahn *et al.*, *Nature (London)* **428**, 401 (2004).
 - [15] P. Littlewood, *Nature (London)* **399**, 529 (1999); V. Podzorov *et al.*, *Phys. Rev. B* **64**, 140406 (2001); V. Hardy *et al.*, *ibid.* **69**, 020407(R) (2004).